RMetS

Royal Meteorological Society

Monitoring and forecasting drought impact on dryland farming areas

Saleh Arshad,[a] Saeed Morid,[a]* Mohammad Reza Mobasheri,[b] Majid Agha Alikhani[a]
and Sajjad Arshad[c]

[a] *College of Agriculture, Tarbiat Modares University, P.O. Box 14115-336, Teheran, Iran*
[b] *International Water Management Institute, P.O. Box 2075, Colombo, Sri Lanka*
[c] *College of Computer, Shahid Beheshti University, Teheran, Iran*

ABSTRACT: Frequent drought amplifies the need for a warning system and forecasting models for damage to crop yields. This study developed an operational model to assess agricultural drought impact. The dryland areas of Kermanshah Province (Iran) were selected to test the proposed modelling system. The model predicted the consequences of drought damage on wheat crop during critical stages of growth (emergence, vegetative growth, initiation of flowering, grain filling, and maturity) as a drought loss indicator. Two types of input were evaluated to correlate climate conditions *versus* drought losses. The first group comprises the Palmer Drought Severity Index, Z-index, Crop Moisture Index, Crop-Specific Drought Index (CSDI), Standardized Precipitation Index, and Effective Drought Index with one- to three-month timescales used as meteorological indices. The second group, which is consistent of the vegetation condition index and temperature condition index, is based on satellite data. Also a new satellite-based version of CSDI, so-called standardized CSDI (S-CDSI), where evapotranspiration was estimated using surface energy balance algorithm for land, is used. Adaptive Neuro-Fuzzy Inference Systems (ANFIS) technique was used for forecasting with genetic algorithms applied to select appropriate inputs from among the large number of indices. It was concluded that the combination of meteorological and satellite indices performed best in forecasting crop yield. As expected, accuracy improved over the growth stages as the crop developed. Enhancement of the model with a GIS platform made it possible to present the results more suitably, hence helping users to make more realistic decisions. Copyright © 2012 Royal Meteorological Society

KEY WORDS   agricultural drought; drought losses; satellite data; ANFIS; Iran

Received 6 December 2011; Revised 4 July 2012; Accepted 14 July 2012

1. Introduction

Drought is a temporary and recurring meteorological event and the agricultural sector is the main victim of this natural disaster. Agricultural drought is mainly the result of precipitation shortages, differences between actual and potential evapotranspiration (ET), and soil water deficits. Thus, drought impact also varies according to prevailing weather conditions, biological characteristics of the crops, and their growth stages.

To cope with drought and reduce consequent losses, it is crucial to develop a warning system to forecast potential drought impact on final agriculture production at the preplanting and early crop-growth stages using a number of indicators. Such a system allows decision makers sufficient time to implement strategies to reduce risk potential. The main indicators for drought monitoring are drought indices, which can be used to quantify the moisture condition of a region and detect the onset and severity of a drought and the spatial extent of a

drought event that allows comparison of moisture supply conditions between regions (Alley, 1984).

Many drought indices have been developed to date. These include the Palmer Drought Severity Index (PDSI; Palmer, 1965), which is widely used in the USA, the Deciles Index (Gibbs and Maher, 1967), which is operational in Australia, Crop Moisture Index (CMI), which uses a meteorological approach to monitor week-to-week crop conditions (Palmer, 1968), Standardized Precipitation Index (SPI; McKee *et al.*, 1993), which has gained the world popularity, Effective Drought Index (EDI) attempt to more accurately determine the exact start and end of a drought period with a daily time step (Byun and Wilhite, 1999), and so on. A review of drought indices can be found in several sources, including Smakhtin and Hughes (2007) and Morid *et al.* (2006).

Correlating drought indices and crop performance to assess the impact of drought has been the focus of a number of studies. Quiring and Papakryiakou (2003) evaluated the PDSI, Z-index, SPI, and NOAA drought index (NDI) to measure agricultural drought. Wu and Wilhite (2004) developed an agricultural drought risk assessment model based on variables derived from SPI and CDSI using multivariate regression techniques. In

* Correspondence to: S. Morid, Tarbiat Modares University, College of Agriculture, P.O. Box 14115-336, Teheran, Iran.
E-mail: morid_sa@modares.ac.ir

another study, Mkhabela *et al*. (2010) identified drought indices that strongly correlated with spring wheat yield and quality. Their results showed that SPI is suitable to be applied as a water supply index. Manatsa *et al*. (2010) also analysed the vulnerability of crops from frequency and spatiotemporal characteristics of agricultural droughts in Zimbabwe using SPI. All these studies took place only in dryland farming areas to prevent the impact of irrigation on soil moisture and crop growth. It should be emphasized that in these studies, a dominant crop was used to evaluate the indices for agricultural drought monitoring (e.g. wheat in Wu and Wilhite, 2004 and Manatsa *et al*., 2010 or barley in Quiring and Papakryiakou, 2003).

From another point of view, in data-sparse regions of the world, monitoring systems are faced with two main limitations: low density of climate observation points and, most importantly, difficulty to provide near-real-time data (Smakhtin *et al*., 2006). Remote sensing (RS) technology is a possible solution to these limitations. Satellite-derived data have the advantages of consistent spatial coverage and near-real-time availability. For these reasons, they are widely used in various aspects of natural resources management, including drought monitoring (Boken *et al*., 2005). Perhaps the most well-known satellite-sensor-derived vegetation index is the normalized difference vegetation index (NDVI) (Rouse *et al*., 1973; Tuker, 1979). Other such indices are the vegetation condition index (VCI) and the NDVI deviation from its long-term mean (DEV) that originated with the NDVI and has been applied for drought monitoring (Thenkabail *et al*., 2004).

Although monitoring can identify the early signs of drought, complimentary analysis is required to forecast its future impact. Such a tool provides information in a timely manner about potential agricultural drought risks to allow decision makers and farmers to adopt relevant measures. An intelligent computing tool, the adaptive neuro-fuzzy inference system (ANFIS), is a hybrid approach that is proven to be efficient for forecasting. The main advantages of the method are that it does not require the model structure to be known a priori and it has the ability to handle large amounts of noisy data from dynamic and nonlinear systems, especially when the underlying physical relationships are not fully understood (Nayak *et al*., 2004).

The current study aims to develop an operational modelling system for monitoring and forecasting drought impact on the agriculture sector. The dryland farming area of Kermanshah Province in Iran, where wheat is the major crop, was selected to test the proposed methodology.

2. Materials and methods

2.1. Study area and data

The Kermanshah Province with an area of 24 980 km^2 is located in the western part of Iran (Figure 1). The Province includes 11 provincial cities (PCs) – administrative subdivisions, which are used in this study as the basic geographical unit (Figure 1). The Province is mainly mountainous and is a part of Zagross Ranges. The region's precipitation varies from 375 mm to 575 mm. Figure 2 shows the trend of precipitation time series at Kermanshah Province. The agricultural area covers a total area of about 820 000 ha of the Province (32.81%) and
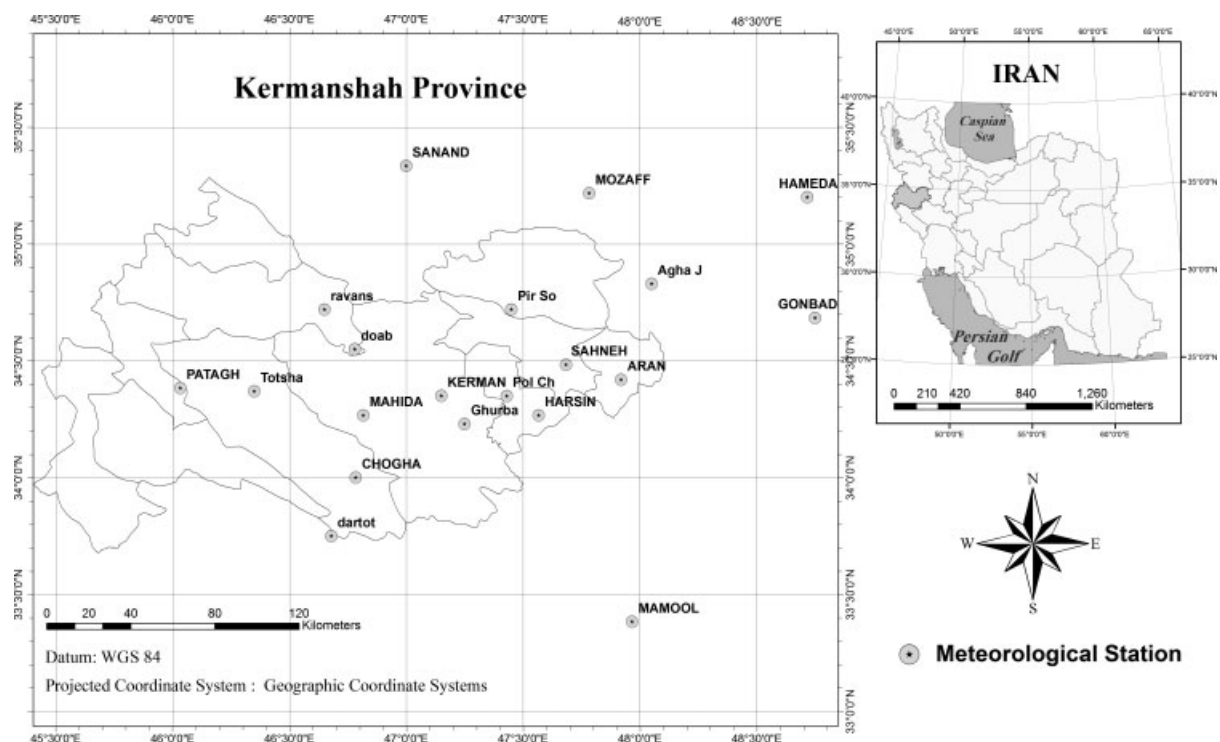

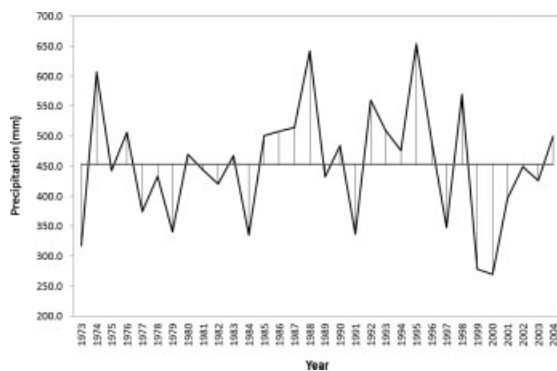Figure 1. Locations of Kermanshah Province meteorological stations.

Figure 2. The trend of precipitation time series at Kermanshah Province.

dryland farming reaches more than 620 000 ha (75.61%). For studies of areal drought extent, the precipitation records from 20 stations in the Province were utilized (Figure 1). The record length at these stations is from January 1974 to December 2004. The missing data is less than 10% and the gaps were patched using regression equations with the nearest suitable station.

The soil data and records of wheat production in the dryland areas within each PC are collected from the Ministry of Agriculture. The available record for the crop yields is from 1984 to 2004. There is also an agrometeorological station in the region (Sara Rud station) that records phonological too. Its data is used to indicate phonological stages of wheat in the study area.

The AVHRR satellite covers the globe twice a day with a spatial resolution of 1.1×1.1 km^2. The sensor collects the radiance data in five spectral bands (band 1: 0.63 μm; band 2: 0.85 μm; band 3: 1.607 μm; band 4: 10.82 μm; band 5: 12.0 μm). The AVHRR images were collected and preprocessed for this study, for an 18 year period, from 1989 to 2007. This period includes one of the recent catastrophic drought spell of 1998–2001, which has been identified as the most severe drought event of the last 35 years (Morid *et al.*, 2007) and ensures that the minimum NDVI is present in the time series of images.

The growing season in the Province is from March to July; hence, the images were selected only from these months. Overall, excluding the cloudy days, 271 images were prepared for this study. Preprocessing of the NDVI images included derivation of maximum value composite (MVC) and extraction of NDVI–MVC values for the PCs within the study time period. The MVC technique retains the highest NDVI value for each pixel during the growing stage periods producing images that are spatially continuous and relatively cloud-free, with temporal resolution sufficient for evaluating vegetation dynamics.

2.2. Meteorological drought indices

For this study, the meteorological drought indices selected are PDSI, Z-Index, CMI, Crop-Specific Drought Index (CSDI), SPI, and EDI, which are among the most frequently recommended for this type of analysis (Quiring and Papakryiakou, 2003; Morid *et al.*, 2007).

2.2.1. PDSI and moisture anomaly index

The *PDSI* and *the Z-index* were both developed by Palmer (1965). The Z-index is a measure of the monthly moisture anomaly and it reflects the departure of moisture conditions in a particular month from normal (or climatically appropriate) moisture conditions (Heim, 2002). PDSI aims to measure moisture conditions that are standardized so that comparisons using the index could be made between locations and between months. The index is based on the supply-and-demand concept of the water balance equation including ET, soil recharge, runoff, and moisture loss from the surface layer.

2.2.2. Crop moisture condition

The *CMI*, also developed by Palmer (1968), is a complement to the PDSI. It measures the degree to which crop moisture requirements are met. It is more responsive to short-term changes in moisture conditions and is not intended to assess long-term droughts.

2.2.3. Crop-Specific Drought Index

The *CSDI* (Meyer *et al.*, 1993) is one of the rare indices that incorporate directly ET in drought monitoring. It is based on the ratio of actual ET to potential ET:

$$\text{CSDI} = \prod_{i=1}^{n} \left(\frac{\sum \text{ET}_{\text{act}}}{\sum \text{ET}_{\text{pc}}} \right)_i^{\lambda_i} \qquad (1)$$

where ET_{act} and ET_{pc} are the actual and the potential ET (mm), respectively, for the crop at each growth period; n is the number of periods chosen to represent the crop's growth cycle; and λ_i is the relative sensitivity of the crop to moisture stress during the ith period of growth. However, in this reach work, similar to Wu and Wilhite (2004), it is assumed to be 1.

2.3. Satellite drought indices

RS-based vegetation indices are radiometric measures of the dynamics of vegetation conditions employing the spectral signatures of canopy elements, particularly in the red and near-infra red portions of the spectrum (Huete *et al.*, 2002). By utilizing reflectance data in two or more spectral bands, these indices can enhance vegetation signals and cancel out the effects of topography, sun angle, and atmosphere.

2.3.1. Normalized difference vegetation index

Perhaps the most well-known satellite-sensor-derived vegetation index at present is NDVI, suggested by Tucker (1979):

$$\text{NDVI} = \frac{(\lambda_{\text{NIR}} - \lambda_{\text{RED}})}{(\lambda_{\text{NIR}} + \lambda_{\text{RED}})} \qquad (2)$$

where λ_{NIR} and λ_{RED} are the reflectance in the NIR and RED bands, respectively. Because of its close relation with vegetation vigour and accessible soil moisture,

NDVI is commonly used in drought studies (Lim and Kafatos, 2002; Olsson *et al.*, 2005).

2.3.2. Vegetation condition index

Another vegetation-related index, which is a derivation of the NDVI, is VCI. Kogan (1995) suggested this index as a measure of difference between present vegetation condition and the worst vegetation condition observed for a long term in the same location:

$$\text{VCI} = \frac{(\text{NDVI} - \text{NDVI}_{min})}{(\text{NDVI}_{max} - \text{NDVI}_{min})} \times 100 \quad (3)$$

where NDVI_{max} and NDVI_{min} are the maximum and minimum values in NDVI time series, respectively. The above indices are assigned threshold values, which reflect vegetation conditions and through it various levels of drought severity (e.g. Thenkabail *et al.*, 2004; Smakhtin *et al.*, 2006).

2.3.3. Temperature crop index (TCI)

TCI (Kogan, 1995) is also applied in this study. The index reflects vegetation's response to temperature (the higher the temperature, the more extreme the drought). The TCI uses brightness temperature and represents the deviation of the current month's (week's) value from the recorded maximum (Thenkabail *et al.*, 2004):

$$\text{TCI} = \frac{(\text{BT}_{max} - \text{BT})}{(\text{BT}_{max} - \text{BT}_{min})} \quad (4)$$

where BT is the weekly (or monthly) smoothed brightness temperature (e.g. AVHRR band 4), BT_{min} and BT_{max} are the minimum and maximum values of BT in a long-term record of RS images for each calendar month or week.

2.3.4. Standardized CSDI (S-CSDI)

As shown before, the CDSI is not satellite based (Equation (1)). However, in this study, the index was modified to be calculated using RS data. For this, the nominator for an equation (ET_{act}) was estimated using the surface energy balance algorithm for land (SEBAL) (Bastiaanssen *et al.*, 1998) that uses satellite images to estimate actual ET and other energy exchanges at the Earth's surface. A further modification relates to the standardization estimation:

$$\text{S-CSDI} = \frac{(\text{CSDI} - \text{CSDI}_{min})}{(\text{CSDI}_{max} - \text{CSDI}_{min})} \times 100 \quad (5)$$

where CSDI_{max} and CDSI_{min} are the maximum and minimum values in the CDSI time series, respectively. This equation makes it possible to compare the present status of water stress with its worth and the best water stress conditions over the long term in the same location (i.e. each pixel of an image). This makes it useful for agricultural drought monitoring in irrigated land, so that case studies would not be limited to rain fed areas, as in the work of Quiring and Papakryiakou (2003), Wu and

Wilhite (2004), and Manatsa *et al.* (2010). Details of this emerging method are available from Arshad (2008).

2.4. SEBAL algorithm

The SEBAL is a parameterization of the energy balance and surface fluxes based on spectral satellite measurements (Bastiaanssen *et al.*, 1998).

$$\lambda_{\text{ET}} = R_n - G - H \quad (6)$$

It requires visible, near-infrared, and thermal-infrared input data (e.g. AVHRR band 1, 2, 4 and 5). Instantaneous net radiation values are computed from incoming solar radiation measured via surface albedo, surface emissivity, and surface temperature.

$$R_n = R_{S\downarrow} - \alpha R_{S\downarrow} + R_{L\downarrow} - R_{L\uparrow} - (1 - \varepsilon_0)R_{L\downarrow} \quad (7)$$

where $R_{S\downarrow}$ is the incoming short-wave radiation (W m^{-2}), α is the surface albedo (dimensionless), $R_{L\downarrow}$ is the incoming long-wave radiation (W m^{-2}), $R_{L\uparrow}$ is the outgoing long-wave radiation (W m^{-2}), and ε_0 is the surface thermal emissivity (dimensionless).

This method computes surface albedo from the top of the atmosphere broadband albedo using an atmospheric correction procedure. Soil heat flux is computed from surface temperature, surface albedo, NDVI, and roughness length derived from the soil adjusted vegetation index (SAVI). The sensible heat flux is determined by an iterative solution of standard heat and momentum transport equations using a pixel-based Monin–Obukhov stability correction. A spatial interpolation technique is applied consecutively to incorporate spatial thermal radiation variations and the effects arising from buoyancy on momentum and sensible heat fluxes. Using thermal band, a wet and a dry pixel are needed for each of satellite images. The sensible heat flux (H) is set to 0 for the wet pixel and to the difference between net radiation and soil heat flux, for the dry pixel. For the dry pixel, it is assumed that dTa (the vertical difference in air temperature) is a function of the sensible heat flux, whereas for the wet pixel, dTa is assumed to be 0. From the dTa and the surface temperature for these two pixels, a linear relationship is assumed and used to compute dTa for the remaining pixels of the image. Sensible heat flux at each pixel is computed from the dTa pixel values and the latent heat flux is found as a residual term. The instantaneous latent heat fluxes are then converted to the required daily ET values by assuming that the instantaneous evaporative fraction is similar over 24 h.

To run the SEBAL model, it was necessary to adjust the accuracy of applied assumptions such as soil heat flux, atmospheric available moisture, and their impact on surface temperature throughout Kermanshah Province. To do this, the soil temperature profile was evaluated to determine the soil heat flux direction. Figure 3 shows soil temperature profiles between 8 a.m. and 1 p.m. at depths of up to 100 cm on 13 June 2007. As shown, the direction of heat flux was upward during the initial hours
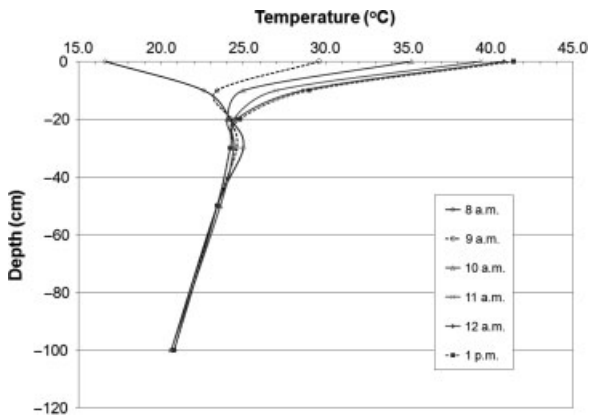
Figure 3. Soil temperature profiles between 8 a.m. and 1 p.m. at depths up to 100 cm on 13 June 2007.

Table I. Dates for phonological stages.

Stage	Period	Date
First	Germination	10th week
Second	Vegetative growth	19th week
Third	Initiation of flowering	20th week
Fourth	Grain filling	22nd week
Fifth	Maturity	25th week

2.5. Critical phonological stages and yield departure

2.5.1. Critical phonological stages

These stages are defined to enable the model to be updated during the growing season. Such an approach is also applied by Wu and Wilhite (2004). For this, five periods are defined for wheat, including vegetative, blooming, pod formation, pod fill, and ripening (Table I and Figure 4). Using the simultaneous weather and phonological data from the Sararud stations, the dates of these periods are calculated based on the growing degree days (GDD). Furthermore, the daily GDD maps are created for the study area and the growth stages are

(8 a.m. curve). However, the negative direction of this flux becomes positive at about 9 a.m. as the sun rose. It is a general pattern, which is also shown in Mobasheri (2007). Thus, heat flux in the energy budget equation is represented by the passage time of the satellite in the SEBAL model.
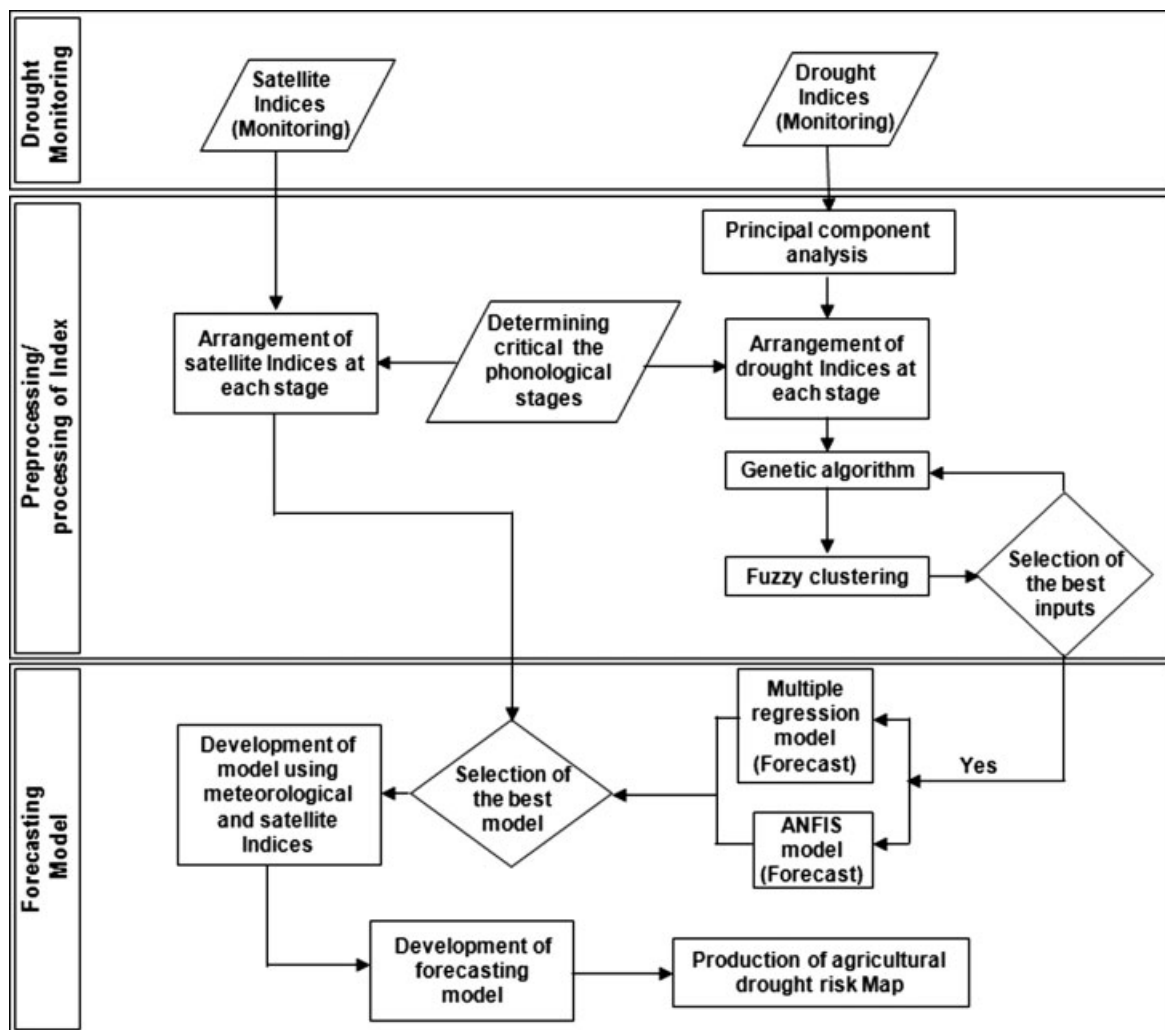

Figure 4. A schematic plot of the growing stages and timing of the forecasting models.

Table II. Categories of agricultural losses (Zhang, 2004).

Yield category	Yield residual
Extreme loss	$>1.17\sigma$
Moderate loss	$1.17\sigma > Y > 0.33\sigma$
Normal	$0.33\sigma > Y > -0.33\sigma$
Moderate increase	$-0.33\sigma > Y > -1.17\sigma$
Extreme increase	$< -1.17\sigma$

Figure 5. Drought risk assessment model formulation methodology.

estimated for each PC, using geographical information system (GIS) capabilities.

2.5.2. Yield departure

As it is expected, there is a positive trend in the 21 years yield data, due to farming innovations. The data are detrended by regressing the average annual yield against the year-of-harvest for each PC (Quiring and Papakyiakou, 2003). The resulting unstandardized residuals (hereafter, referred to as yield departures) are calculated for each PC and used in development and evaluation of the yield models. To apply a standard criterion to indicate risk, five stages are defined based on standard deviation (σ) of the yield departures suggested by Zhang (2004), which is shown in Table II.

2.6. Forecasting model

The multiple regression method and ANFIS model were applied in this study to forecast final crop yield. ANFIS modelling refers to the method of applying various learning techniques developed for training of the artificial neural network (ANN) (Morid *et al.*, 2007) to fuzzy modelling or a fuzzy inference system (FIS) (Brown and Harris, 1994). ANFIS creates an FIS for which membership function parameters are adjusted using either a backpropagation algorithm alone or a combination of this algorithm and a least squares method. In another word, this allows the fuzzy system to learn from the data being modelled. Several types of fuzzy reasoning have been proposed in the literature. This study uses the Sugeno fuzzy model (Takagi and Sugeno, 1983; Sugeno and Kang, 1988) as the consequent part of this FIS is a linear equation and the parameters can be estimated by a simple least squares error method. More details about this technique can be found in (Farokhnia *et al.*, 2010).

3. Results and discussion

A modelling framework was developed as shown in Figure 4, which considered the following characteristics for monitoring and forecasting systems:

- The drought risk assessment was based on the Province's dryland areas and forecasting wheat yield was an indicator of agricultural drought risk. However, it had the capability of being extended to irrigated areas by using S-CSDI.
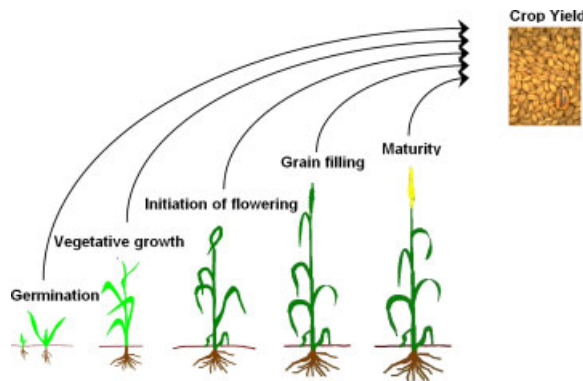
- The system evaluated and integrated the aforementioned meteorological and satellite data indices as moisture supply indicators.
- Intelligent techniques were applied to select the most suitable indices and forecast the final yield.
- The forecasts were done at critical crop times during the growing season and the moisture indicators were updated as the crop grew. Five models were developed to forecast crop production at each growing stage. Figure 5 shows this approach schematically for more clarification.

3.1. Calculating drought indices

The meteorological drought indices were also calculated using the drought index package (DIP) (Morid *et al.*, 2005). These indices were calculated for selected stations and then their respective GIS layers were prepared using inverse distance method that is reported to be suitable to create drought maps (Akhtari *et al.*, 2009). More than 14 000 GIS layers were created and their average values were extracted for each PC. Figure 6 shows a set of drought maps created using the DIP for May 1999.

Figure 7 illustrates the software developed to deal with the large number of images and the preprocessing/processing required for the RS indices. The software was designed to:

- preprocess RS images;
- calculate *ETa* using SEBAL, AVHRR (bands 1, 2, 4, and 5), regional digital elevation model (DEM), land use layer, and synoptic meteorological data of the study area;
- produce drought index maps, including VCI, TCI, ET_{act}, CDSI, and S-CDSI. For example, Figure 8 shows the output of the software for 4 June 2004. The resulting images were then processed to extract their mean values within the boundaries of the PCs for further analysis. These values were the inputs for the forecasting models.

For the initial evaluation of the meteorological and RS indices, their average values in the PCs were correlated
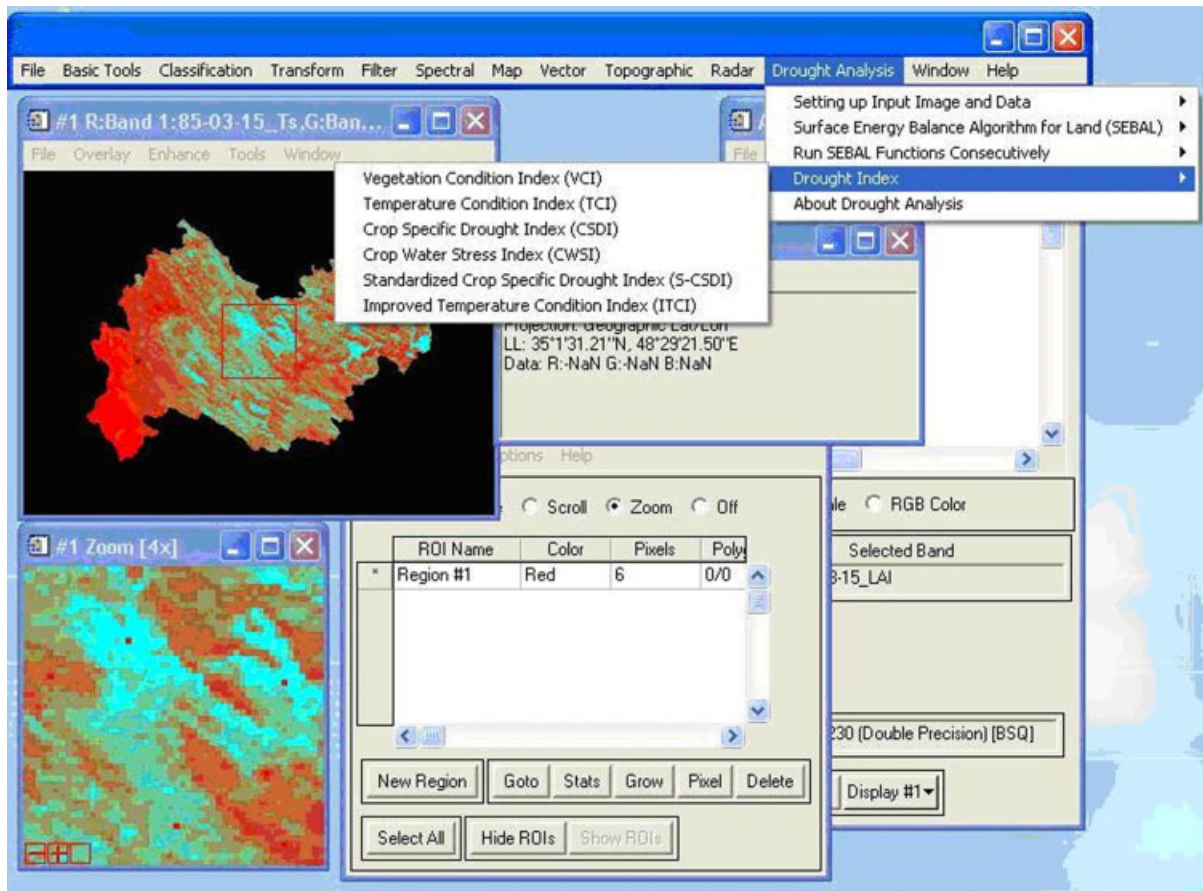
Figure 6. Sample maps of meteorological drought indices for May 1999 (EDI, CMI, SPI, and PDSI).
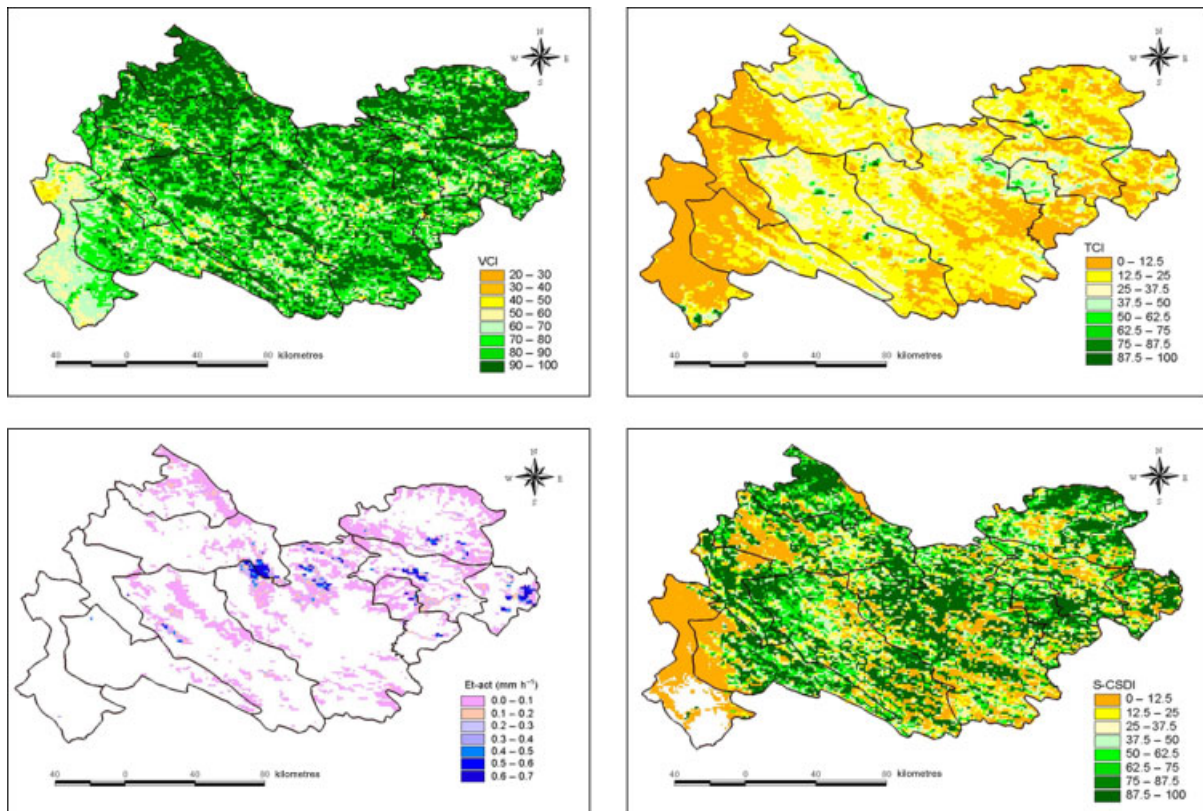

Figure 7. Interface of model software-calculated ETa and images of drought satellite indices.
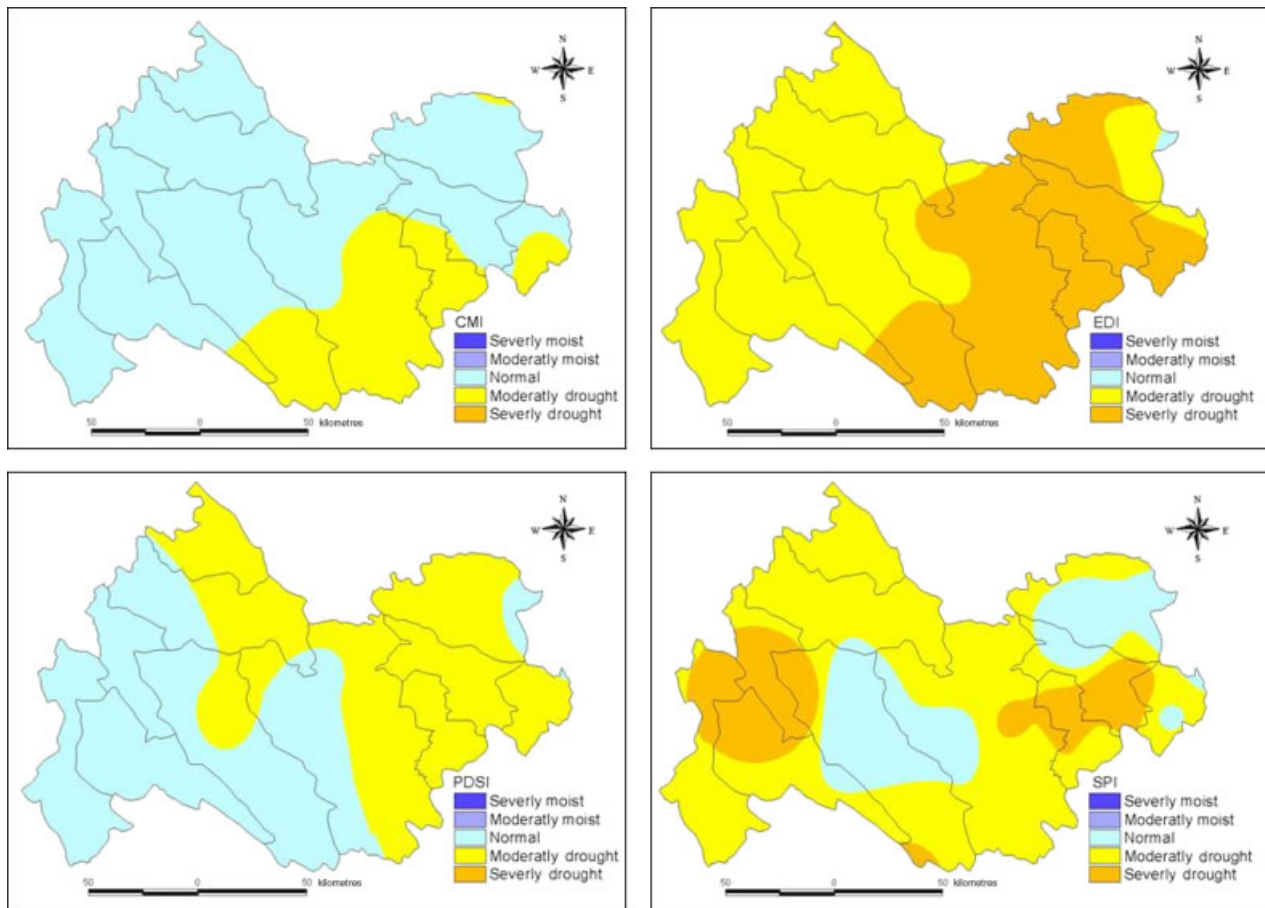
Figure 8. Sample maps of satellite drought indices for 6 June 2004 (VCI, TCI, ETa, and S-CSDI).

against the final yield departure (e.g. 39 year mean values of SPI or VCI vs yield departure). This is done for all growing stages (Tables III and IV). It was seen that the performance of S-CSDI was significantly better than the other indices. For instance, at stage 5, when R^2 for S-CDSI was 0.47, it was 0.38 for SPI and 0.23 for VCI. However, none of the indices were able to forecast yield departure in the first stage (10 weeks after planting or 31 weeks before harvesting).

3.2. General variable selection

The impact of water stress on yield is related to precipitation amount, intensity, timing, and distribution. Drought index values on high-frequency time scales reflect moisture supply more precisely than low-frequency time scales (Wu and Wilhite, 2004). As already described in this study, the meteorological indices were evaluated for both weekly and monthly time scales. Drought maps of the indices were first created and then their mean values were calculated for each PC. These values became inputs for the forecasting models. The number of indices and time scales were excessive and had fewer degrees of freedom. Thus, it was decided to apply principal components analysis, a useful tool to reduce the statistical interdependence of variables and retains most of the variation of the original variables (Meyer *et al.*, 1991).

The values of the satellite drought indices were calculated for each of the five growing stages. For VCI, MVC was applied to get the highest NDVI for each pixel during each growing season and the consequent mean values for the PCs. For TCI, CSDI, and S-CDSI, the average values of the available images for each period were calculated and the average value of each PC was determined.

A reciprocal approach was applied to evaluate and select the selected variables for each of the five growing stages (Table V). In the first step, the best combination of the variables was screened using a genetic algorithm (GA) and an ANN. GA is a search technique used to find exact or approximate solutions to optimization and search problems. In this study, in a two-way process, GA created a population from the variables and the performance of the population was checked by ANN.

In an iterative calculation, the best population (the one that causes the best performance of ANN) evolved. To increase the degrees of freedom of the forecasting model, the population was again screened to reduce the number of variables. This time the variables were selected by stepwise elimination of the nonsignificant variables. The coefficient of determination (R^2) was used to measure the goodness-of-fit of the model (closeness of the relationship between the indices) and the relative yield departure in each PC.

Table III. Performance of CMI, EDI, PDSI, SPI, and Z-Index (ZIND) in forecasting yield departure.

Index*	R^2	MAE	RMSE	d
CMI-1	0.12	25.53	32.67	0.45
CMI-2	0.31	22.73	28.97	0.65
CMI-3	0.47	19.44	25.37	0.79
CMI-4	0.46	19.34	25.76	0.78
CMI-5	0.43	19.42	26.25	0.77
EDI-1	0.06	26.18	33.79	0.33
EDI-2	0.15	25.14	32.20	0.47
EDI-3	0.27	23.38	29.83	0.64
EDI-4	0.30	22.93	29.21	0.67
EDI-5	0.31	22.65	29.11	0.67
PDSI-1	0.08	24.87	33.48	0.37
PDSI-2	0.14	24.51	32.39	0.48
PDSI-3	0.20	23.68	31.19	0.57
PDSI-4	0.20	23.65	31.13	0.57
PDSI-5	0.21	23.40	30.96	0.58
SPI-1	0.06	25.54	33.91	0.29
SPI-2	0.16	25.42	32.03	0.50
SPI-3	0.19	25.06	31.34	0.55
SPI-4	0.32	1.32	2.32	3.32
SPI-5	0.38	20.65	27.42	0.73
ZIND-1	0.12	24.93	32.76	0.40
ZIND-2	0.25	23.63	30.17	0.61
ZIND-3	0.38	21.04	27.53	0.73
ZIND-4	0.35	20.30	28.25	0.70
ZIND-5	0.32	20.74	28.85	0.68

* 1–5 refers to the five phenological stages.

Table IV. Performance of VCI, TCI, and S-CDSI in forecasting yield departure.

Index*	R^2	MAE	RMSE	d
VCI-1	−0.01	30.33	39.73	0.01
VCI-2	0.18	30.43	39.08	0.22
VCI-3	0.49	27.93	34.69	0.60
VCI-4	0.32	29.41	37.64	0.39
VCI-5	0.23	29.13	38.65	0.27
TCI-1	−0.08	42.88	51.78	0.42
TCI-2	0.48	27.65	34.83	0.58
TCI-3	0.08	30.27	39.61	0.08
TCI-4	0.26	30.36	38.41	0.30
TCI-5	−0.02	30.37	39.72	0.02
S-CSDI-1	0.09	29.98	39.55	0.12
S-CSDI-2	0.58	25.41	32.27	0.71
S-CSDI-3	0.67	24.20	29.49	0.78
S-CSDI-4	0.60	24.82	31.75	0.71
S-CSDI-5	0.47	27.49	34.99	0.58

* 1–5 refers to the five phenological stages.

This approach to variable selection was repeated for all five stages and the results are shown in Table V. The signs $\sqrt{}$, $+\sqrt{}$, and $++\sqrt{}$ in the table refer to the initial, GA–ANN, and stepwise elimination selections, respectively.

3.3. Development of the forecasting model

To train the purposed ANFIS models, the early stopped training approach (STA) that is discussed by Coulibaly *et al.* (2000) is applied. For this the available data are split in to three parts: (1) a training set, used to determine the network weights; (2) a validation set, used to estimate the network performance and decide when we stop training; and (3) an eradication (or test), used to verify the effectiveness of the stopping criterion and estimate the expected performance in the future. Parts (1) and (2) are considered together as the calibration period and Part (3) as the test period. To check ability of the ANFIS model, its results are also compared with multiple regression technique (MRT).

3.4. Evaluating forecasting models

The performances of the forecasting models were evaluated using R^2, residual mean square error (RMSE), and an agreement index (d) (Quiring and Papakryiakou, 2003). The best performance yields R^2 and d equal to 1 and *RMSE* equal to 0.

The evaluation was done in two steps. First, the performances were evaluated solely by the meteorological drought indices (dataset 1) (Table VI). The objective was mainly to compare the results of the ANFIS and MRT models. Table VI shows that ANFIS performed better. This was more pronounced for R^2 and d. For instance, R^2 at the fifth stage reached 0.73 for ANFIS and 0.54 for MRT. Poor performance in predicting crop yield in the first growing stage was a common weakness for both models. However, especially for ANFIS, the results progress and were more reliable after the second stage.

In the second step, the performance of ANFIS was evaluated using satellite indices (dataset 2) and a combination of satellite and meteorological indices (dataset 2) as inputs (Table VII). This evaluation made it possible to compare these results with previous results (Table VI, ANFIS column). Comparison of the two tables reveals that the ANFIS model had a similar impact on datasets 1 and 2. For instance, at stage 5, R^2, d, and RMSE for dataset 1 were 0.73, 0.89, and 33.09, respectively, and for dataset 2 were 0.74, 0.86, and 36.91, respectively. A combination of the first two datasets (dataset 3) improved results significantly (Table VII). Notably, R^2, d, and RMSE were 0.81, 0.94, and 38.57, respectively. This improvement was observed in other stages also. The first stage was less reliable than the other datasets. It is worth mentioning that the values shown in Tables VI and VII are from the testing period and results in the calibration period were much better.

The drought of 1999 was one of the worst in the past 30 years, with rainfall deficits consistently of more than 40% of the mean annual rainfall. The severity of this drought placed extreme strain on the water resources and agriculture of the study area. Figure 9(a)–(c) shows forecasts from ANFIS using dataset 3 in a GIS platform.

Table V. Variables used in discriminate analysis at each critical phonological stage for dryland wheat.

Variables (STB)	St.1	St.2	St.3	St.4	St.5	Variables (STB)	St.1	St.2	St.3	St.4	St.5	Variables (SB)	St.1	St.2	St.3	St.4	St.5
Third month's SPI	√+	–	–	–	–	23rd week's Z-index	–	–	–	–	√++	VCI-stage 1	√	–	–	–	–
Third month's PDSI	√	–	–	–	–	24th week's CMI	–	–	–	–	√	VCI-stage 2	–	√	–	–	–
Third month's Z-index	√	–	–	–	–	24th week's Z-index	–	–	–	–	√+	VCI-stage 3	–	–	√	–	–
Third month's SPI-3	√++	√++	√++	–	–	25th week's CMI	–	–	–	–	√+	VCI-stage 4	–	–	–	√	√
Third month's PDSI-3	√	–	–	–	–	25th week's Z-index	–	–	–	–	√	VCI-stage 5	–	–	–	–	–
Third month's Z-index-3	√++	√++	–	–	–	Fifth month's SPI	–	–	–	–	√	TCI-stage 1	√	–	–	–	–
19th week's CMI	–	√	–	–	–	Fifth month's Z-index	–	–	–	–	–	TCI-stage 2	–	√	–	–	–
19th week's PDSI	–	√	–	–	–	First PC of third month	√+	–	–	–	–	TCI-stage 3	–	–	√	–	–
19th week's Z-index-I	–	√	–	–	–	Second PC of third month	√++	–	–	–	–	TCI-stage 4	–	–	–	√	√
19th week's EDI	–	√+	√+	–	–	Third PC of third month	√	–	–	–	–	TCI-stage 5	–	–	–	–	–
5th month's SPI	–	√+	–	–	–	First PC of 19th week	–	√	–	–	–	CSDI-stage 1	√	–	–	–	–
Fifth month's PDSI	–	√++	√++	–	–	Second PC of 19th week	–	√	–	–	–	CSDI-stage 2	–	√	–	–	–
Fifth month's Z-index	–	–	√+	√++	√++	Third PC of 19th week	–	√	√+	–	–	CSDI-stage 3	–	–	√	–	–
20th week's CMI	–	–	√	√++	–	First PC of fifth month	–	√	√+	–	–	CSDI-stage 4	–	–	–	√	√
20th week's PDSI	–	–	√	–	–	Second PC of fifth month	–	–	√+	–	√++	CSDI-stage 5	–	–	–	–	–
20th week's Z-index	–	–	√	–	–	Third PC of fifth month	–	–	√	–	–	S-CSDI-stage 1	√	–	–	–	–
20th week's EDI	–	–	–	√	√	First PC of 20th week	–	√	√	–	–	S-CSDI-stage 2	–	√	–	–	–
22nd week's CMI	–	–	–	√	√+	Second PC of 20th week	–	√	–	–	–	S-CSDI-stage 3	–	–	√	–	–
22nd week's PDSI	–	–	–	√+	√	Third PC of 20th week	–	–	√	–	–	S-CSDI-stage 4	–	–	–	√	–
22nd week's Z-index	–	–	–	–	√	First PC of 22nd week	–	–	–	√	–	S-CSDI-stage 5	–	–	–	–	–
22nd week's EDI	–	–	–	–	–	Second PC of 22nd week	–	–	–	√+	–	–	–	–	–	–	–
23rd week's CMI	–	–	–	–	√++	Third PC of 22nd week	–	–	–	√	√++	–	–	–	–	–	–

Initial variables √.
Step 1: Selected variables by GA–ANN √+.
Step 2: Selected variables by Stepwise Reg. √++.
St. = Stage.
PC refers to principal analysis components.

Table VI. Performance of multiple regression and ANFIS models using meteorological indices (dataset 1) for dryland wheat production forecasts.

Model	Multiple regression			ANFIS		
	R^2	d	RMSE	R^2	d	RMSE
Growth stage 1	0.24	0.39	44.11	0.29	0.55	50.64
Growth stage 2	0.42	0.71	36.53	0.67	0.83	36.31
Growth stage 3	0.34	0.67	32.75	0.67	0.90	35.46
Growth stage 4	0.51	0.80	35.16	0.73	0.90	39.08
Growth stage 5	0.54	0.83	33.23	0.73	0.89	33.09

Table VII. Performance of ANFIS models using satellite indices (dataset 2) and combined indices (dataset 3) for dryland wheat production forecasts.

Model	Satellite indices			Combined indices		
	R^2	d	RMSE	R^2	d	RMSE
Growth stage 1	0.29	0.55	50.64	0.47	0.65	45.94
Growth stage 2	0.67	0.83	36.31	0.73	0.71	59.10
Growth stage 3	0.75	0.90	35.46	0.83	0.95	26.05
Growth stage 4	0.73	0.90	39.08	0.74	0.91	34.93
Growth stage 5	0.78	0.92	33.09	0.81	0.94	28.57

Similarly, the figure shows better performance of the ANFIS model with dataset 3.

Another approach applied to evaluate yield forecasts uses the following ranking:

Rank 1 = model estimated class of yield loss/increase equals real condition (perfect forecast).

Rank 2 = model correctly predicted the loss, but the intensity was different.
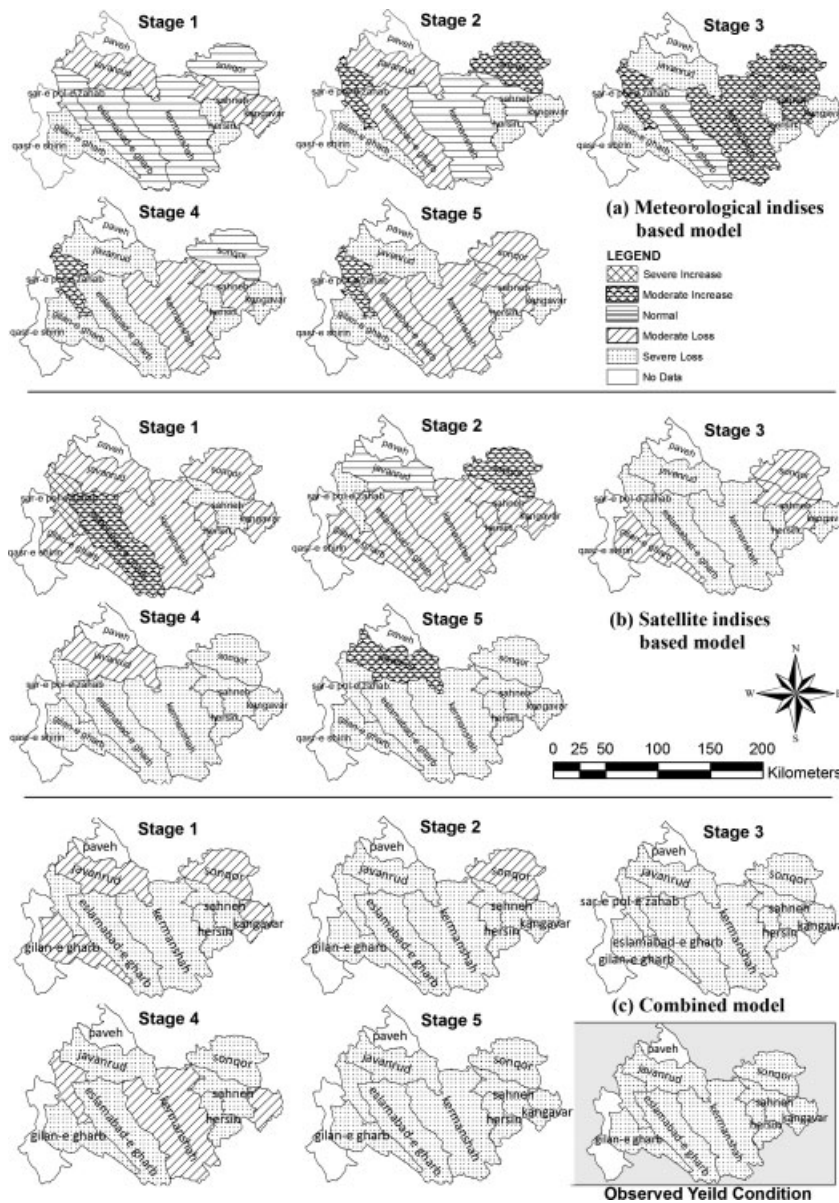

Figure 9. Performance of forecasting models for agricultural loss from 1999 drought.

Rank 3 = model predicted loss/increase in production under normal condition.

Rank 4 = model predicted loss/increase in production that was the reverse of the real condition (worst forecast).

A comparison of the ranking system is shown in Figure 10. An increase in frequency rank 1 (the most favorable forecast) and a decrease in rank 4 (the worst forecast) can be observed for dataset 3.

4. Conclusion

This study developed an agriculture drought risk assessment model facilitated by a near-real-time monitoring system with impact prediction capabilities. The model forecasted possible losses due to agricultural drought on dryland wheat within the study area by retaining previous and adding current meteorological and satellite information. The critical times were before and during the growing season. Following conclusions were drawn from this study:

- CMI meteorological index had the best performance in forecasting the final crop yield, followed by EDI, SPI, and PDSI.
- S-CDSI, introduced in this study, showed the best results for monitoring of drought losses. An advantage of this index is the capability to be used for irrigated land. VCI and TCI were next best indices.
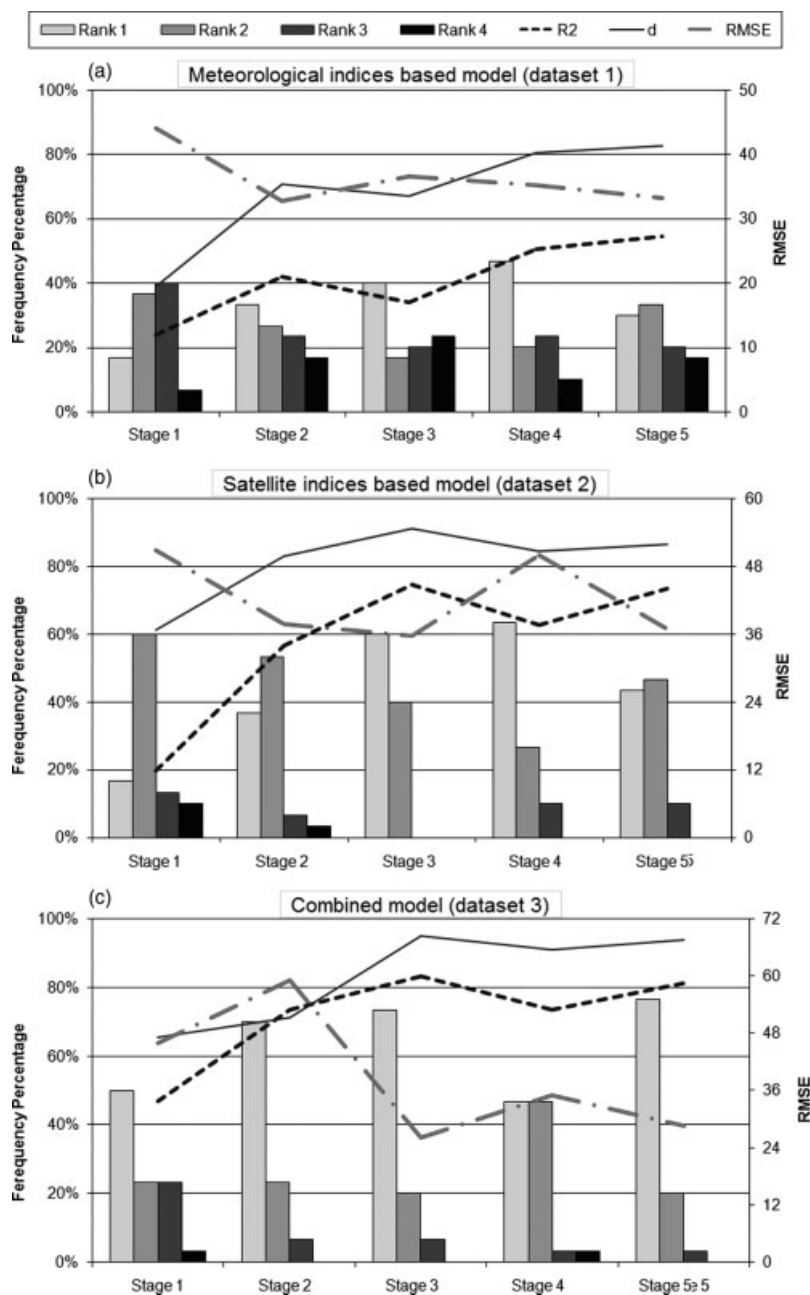

Figure 10. Performance of forecasting models using proposed ranking criteria.

- The combined GA–ANN algorithm and stepwise regression was effective for selecting suitable input variables for the forecasting model. The results showed that the integration of the meteorological and satellite drought indices for multiple time scales described features of moisture supply and vegetation cover affecting the final crop yield before and during the growing season.

- Multiple regression and ANFIS models were applied and the results showed the superiority of the ANFIS model in forecasting the drought impact on the final yield.

- In general, forecast accuracy improved as the growth stages progressed, which is due to getting more updated and effective data. In early May, when the wheat was in bloom, assessment accuracy improved significantly.

- The model accomplished the goal of assessing drought risk on dryland wheat well ahead of harvest, which can be an indicator of the status of other crops. This information can be applied by farmers, decision makers, insurance companies, and the ministries of agriculture and trade to implement necessary actions to mitigate drought impact and food security.

- Applying images with higher resolutions (e.g. LANDSAT) can improve the model performance.

- The methodology of this study is suitable for many areas. The main input is rainfall that is available in many places or even can be prepared from global databases such as PERSSIAN, CRU, or GCPC. The satellite images are also freely available. The phenological information can be also prepared from agricultural stations or even estimated by experts' judgements.

Acknowledgements

References

Akhtari R, Morid S, Mahdian MH, Smakhtin V. 2009. Assessment of areal interpolation methods for spatial of SPI and EDI drought indices. *International Journal of Climatology* 29: 135–145.

Alley WM. 1984. The Palmer Drought Severity Index: limitation and assumptions. *Journal of Climate and Applied Meteorology* 23: 1100–1109.

Arshad S. 2008. *Development of Agricultural Drought Risk Assessment Model, using Satellite Data*, PhD dissertation, Tarbit Modares University, Iran.

Bastiaanssen WGM, Menenti M, Feddes RA, Holtslag AAM. 1998. A remote sensing surface energy balance algorithm for land (SEBAL), 1. Formulation. *Journal of Hydrology* 212–213: 198–212.

Boken VK, Cracknell AP, Heathcote RL. 2005. *Monitoring and Predicting Agricultural Drought*. Oxford University Press: New York, 472.

Brown M, Harris C. 1994. *Neurofuzzy Adaptive Modeling and Control*. Prentice Hall. IFAC workshop on AI in Real-Time Control: Valencia, pp. 213–218.

Byun HR, Wilhite DA. 1999. Objective quantification of drought severity and duration. *Journal of Climate* 117(6): 935–943.

Coulibaly P, Anctil F, Bobee B. 2000. Daily reservoir inflow forecasting using artificial neural networks with stopped training approach. *Journal of Hydrology* 230: 244–257.

Farokhnia A, Morid S, Byun HR. 2010. Application of global SST and SLP data for drought forecasting on Tehran plain using data mining and ANFIS techniques. *Theoretical and Applied Climatology*. DOI: 10.1007/s00704-010-0317-4.

Gibbs WJ, Maher JV. 1967. *Rainfall deciles as drought indicators*. Bureau of Meteorology bulletin No. 48, Commonwealth of Australia. Melbourne: 29.

Heim Jr RR. 2002. A review of twentieth-century drought indices used in the United States. *Bulletin of the American Meteorological Society* 83: 1149–1165.

Huete A, Didan K, Miura T, Rodriguez EP, Gao X, Ferreira LG. 2002. Overview of the radiometric and biophysical performance of the MODIS vegetation indices. *Remote Sensing of Environment* 83: 195–213.

Kogan FN. 1995. Droughts of the late 1980s in the United States as derived from NOAA polar-orbiting satellite data. *Bulletin of the American Meteorological Society* 76: 655–668.

Lim C, Kafatos, M. 2002. Frequency analysis of natural vegetation distribution using NDVI/AVHRR data from 1981 to 2000 for North America: correlations with SOI. *International Journal of Remote Sensing* 23: 3347–3383.

Manatsa D, Mukwada G, Siziba E, Chinyanganya T. 2010. Analysis of multidimensional aspects of agricultural droughts in Zimbabwe using the Standardized Precipitation Index (SPI). *Theoretical and Applied Climatology* 102: 287–305.

McKee TB, Doesken NJ, Kleist J. 1993. The relationship of drought frequency and duration to time scales. In *Proceedings of the Eighth Conference on applied Climatology*. American Meteorological Society: Boston, 179–184.

Meyer SJ, Hubbard KG, Wilhite DA. 1991. The relationship of climatic indices and variables to corn (maize) yields: a principal components analysis. *Agricultural and Forest Meteorology* 55: 59–84.

Meyer SJ, Hubbard KG, Wilhite DA. 1993. A crop-specific drought index for corn: I. Model development and validation. *Agronomy Journal* 86: 388–395.

Mkhabela M, Bullock P, Gervais M, Finlay G, Sapirstein H. 2010. Assessing indicators of agricultural drought impacts on spring wheat yield and quality on the Canadian prairies. *Agricultural and Forest Meteorology* 150: 399–410.

Mobasheri MR. 2007. Uncertainties in the calculation of soil heat flux and sensible heat flux in SEBAL. In *Proceedings of the 2nd Göttingen GIS and Remote Sensing, Göttingen, Germany*.

Morid S, Moghaddasi M, Arshad S, Omid M. 2005. *Manual of Drought Index Package*. The Ministry of Energy: Tehran, Iran.

Morid S, Smakhtin V, Moghaddasi M. 2006. Comparison of seven meteorological indices for drought monitoring in Iran. *International Journal of Climatology* 26: 971–985.

Morid S, Smakhtin VU, Bagherzadeh K. 2007. Drought forecasting using Artificial Neural Networks and time series of drought indices. *International Journal of Climatology* 27(15): 2103–2111.

Nayak PC, Sudheer KP, Rangan DM, Ramasastri KS. 2004. A neurofuzzy computing technique for modeling hydrological time series. *Journal of Hydrology* 291: 52–66.

Olsson L, Eklundh L, Ardo, J. 2005. *A Recent Greening of the Sahel – Trends, Patterns and Potential Causes*. Centre for Environmental Studies, Lund University, Department of Physical Geography and Ecosystem Analysis: Sweden, 12.

Palmer WC. 1965. Meteorological drought. Research paper No. 45. US Weather Bureau: Washington DC.

Palmer WC. 1968. Keeping track of crop moisture conditions, Nationwide: the Crop Moisture Index. *Weatherwise* 21: 156–161.

Quiring SM, Papakryiakou TN. 2003. An evaluation of agricultural drought indices for the Canadian prairies. *Agricultural and Forest Meteorology* 1: 46–62.

Rouse JW, Haas RH, Schell JA, Deering DW. 1973. Monitoring the vernal advancement and retrogradation (green wave effect) of natural vegetation. Progress Report RSC 1978-1, Remote Sensing Center, Texas A&M University, College Station.

Smakhtin VU, Thenkabail P, Gamage N. 2006. Developing on-line near-real time drought monitoring system for southwest Asia. In *Agro-meteorological monitoring in Russia and Central Asian Countries*, Savin I, Negre T (eds). European Commission, Directorate General Joint Research Center, Institute for the Protection and Security of Citizen (IPSC): Istra, Italy, 104–118.

Smakhtin VU, Hughes DA. 2007. Automated estimation and analyses of drought characteristics from monthly rainfall data. *Environmental Modelling & Software*. **22**(6): 880–890.

Sugeno M, Kang GT. 1988. Structure identification of fuzzy model. *Fuzzy Sets and Systems* **28**: 15–33.

Takagi T, Sugeno M. 1983. Derivation of fuzzy control rules from human operator's control actions. In Proc. IFAC Symp. Fuzzy Inform, Knowledge Representation and Decision Analysis. 55–60.

Thenkabail PS, Gamage MSDN, Smakhtin VU. 2004. The use of remote sensing data for drought assessment and monitoring in Southwest Asia. IWMI Research Report No.85. CGIAR: Colombo, Sri Lanka.

Tucker CJ. 1979. Red and photographic infrared linear combinations for monitoring vegetation. *Remote Sensing of Environment* **8**: 127–150.

Wu H, Wilhite DA. 2004. An operational agricultural drought risk assessment model for Nebraska, USA. *Natural Hazards* **33**: 1–21.

Zhang J. 2004. Risk assessment of drought disaster in the maize-growing region of Songliao Plain, China. *Agriculture, Ecosystems and Environment* **102**: 133–153.